


Evolution of ferromagnetism and electron correlation in $\text{Eu}_{1-x}\text{Gd}_x\text{TiO}_3$ thin films with $4f^7$ configuration

N. Takahara ^{1,2,*}, K. S. Takahashi,² Y. Tokura,^{1,2,3} and M. Kawasaki^{1,2}

¹*Department of Applied Physics and Quantum-Phase Electronics Center (QPEC), University of Tokyo, Tokyo 113-8656, Japan*

²*RIKEN Center for Emergent Matter Science (CEMS), Wako 351-0198, Japan*

³*Tokyo College, University of Tokyo, Tokyo 113-8656, Japan*



(Received 28 March 2023; accepted 29 August 2023; published 22 September 2023)

We have studied magnetic and transport properties of compressively strained $\text{Eu}_{1-x}\text{Gd}_x\text{TiO}_3$ (EGTO) thin films up to a high doping level, $x = 0.55$, grown by gas-source molecular beam epitaxy. In comparison with a nonmagnetic dopant (La^{3+}) in $\text{Eu}_{1-x}\text{La}_x\text{TiO}_3$ (ELTO), Gd^{3+} has the same $4f^7$ moment as Eu^{2+} , but a smaller ionic radius to induce buckling of the TiO_6 octahedra and hence reduces the one-electron bandwidth. The evolution of ferromagnetism and electron correlation is more clearly observed in EGTO thin films in the filling (x) dependence of Curie temperature and the coefficient of temperature-squared resistivity. The systematic comparison of the magnetic phase diagrams for EGTO and ELTO has revealed significant differences caused by the presence (absence) of a magnetic moment in Gd^{3+} (La^{3+}) and an effect due to the difference in electron correlation strength.

DOI: [10.1103/PhysRevB.108.125138](https://doi.org/10.1103/PhysRevB.108.125138)

I. INTRODUCTION

Perovskite $3d$ transition metal oxide $\text{ABO}_{3+\delta}$ ($A = \text{Alkali metal, alkaline-earth metal and rare-earth elements}$, $B = 3d$ transition metal elements) has attracted much attention due to its intriguing properties originating from strong electron correlation such as high-temperature superconductivity in cuprates and colossal magnetoresistance in manganite [1]. Rare-earth titanate RTiO_3 ($R = \text{rare-earth elements, Y}$) is one of the simple and prototypical examples of a Mott insulator due to the strong electron correlation of titanium $3d$ -electrons with a t_{2g} orbital character. For example, a metal-insulator transition in $\text{Sr}_{1-x}\text{R}_x^{3+}\text{TiO}_3$ solid solution has been investigated intensively to examine the evolution of electron correlation by controlling the band filling between d^0 and d^1 on the titanium site as well as the band width with various ionic radii of R^{3+} [1–6]. For $\text{Sr}_{1-x}\text{La}_x^{3+}\text{TiO}_3$ with nonmagnetic R , it was reported that the effective electron mass shows a dramatic increase as the system approaches the Mott insulator at $x = 1$ due to electron correlation as revealed by magnetic susceptibility and electronic specific heat [2]. In this study, we employ a Gd^{3+} dopant while keeping the $4f^7$ configuration on the magnetic R -sites in the form of $\text{Eu}_{1-x}\text{Gd}_x^{3+}\text{TiO}_3$ (EGTO).

In addition to band filling, another important factor is the one-electron band width depending on the buckling angle of TiO_6 octahedra [7], which can be controlled by an A -site ionic radius (r_A) as schematically illustrated in Fig. 1(a). As r_A decreases from $R = \text{La}$ to Lu or Y , the bond angle of Ti-O-Ti decreases [7], resulting in a decrement in the transfer integral or band width of the titanium t_{2g} -band [8,9]. For

example, the reported Hubbard gap for LaTiO_3 ($r_A = 1.03 \text{ \AA}$) [9] is as small as 0.2 eV, and a transition to the metallic state takes place at a hole doping of only 5% by strontium substitution ($x = 0.95$) [2,10], while GdTiO_3 ($r_A = 0.93 \text{ \AA}$) exhibits a much larger Hubbard gap of 0.7 eV [11–13], and 20% hole doping ($x = 0.8$) is needed for the insulator-to-metal transition [4,14]. It is noteworthy that r_A also influences the magnetic ground state of the localized Ti^{3+} moment [15–18]. For RTiO_3 with larger r_A for $R = \text{La}, \dots, \text{Sm}$, the Ti^{3+} moments show antiferromagnetic ordering, while showing ferromagnetic ordering for $R = \text{Gd}, \dots, \text{Lu}$ or Y with smaller r_A . Such a magnetic transition is attributed to the fact that the smaller Ti-O-Ti bond angle makes a larger hybridization between the t_{2g} and e_g orbitals at adjacent titanium sites, which enlarges the energetic gain for the ferromagnetic spin configuration rather than the antiferromagnetic one [17]. For example, LaTiO_3 shows G-type antiferromagnetic ordering at a Néel temperature of $T_N = 140 \text{ K}$ [15,18], while GdTiO_3 shows ferrimagnetic ordering at a Curie temperature of $T_C = 30 \text{ K}$, where a localized magnetic moment of Ti^{3+} ($3d^1$) is ferromagnetically ordered and antiferromagnetically coupled with the ferromagnetically ordered magnetic moment of Gd^{3+} ($4f^7$) [15,18].

However, among the series of rare-earth titanates, EuTiO_3 (ETO) is a significant exception because of its valence state, where europium is divalent due to the relatively stable electron configuration of $4f^7$, while titanium is tetravalent with a $3d^0$ configuration. Thus, ETO is a magnetic counterpart of the oxide semiconductor SrTiO_3 (STO), exhibiting G-type antiferromagnetic ordering of Eu^{2+} ($4f^7$) moments at $T_N = 5.5 \text{ K}$ [19–21].

So far, magnetic and transport properties have been investigated for electron-doped ETO mostly by chemical substitution of Eu^{2+} with La^{3+} [22–28], which was motivated by the

*takahara@kws.k.u-tokyo.ac.jp

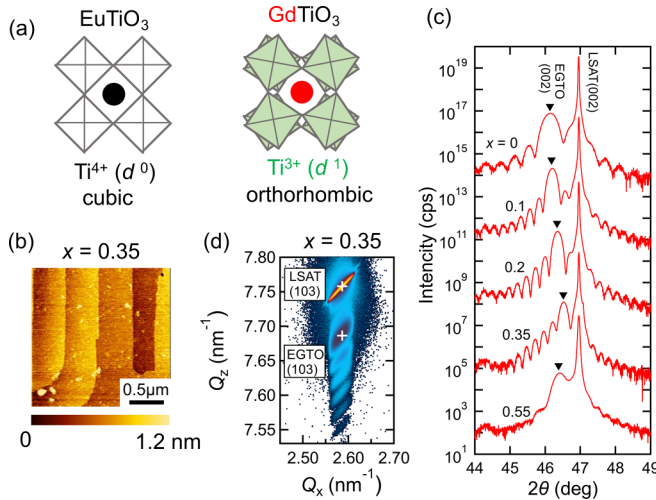


FIG. 1. Structural properties of EGTO thin films grown on LSAT substrates. (a) Schematics of the crystal structures for cubic EuTiO₃ with no distortion (left) and orthorhombic GdTiO₃ with GdFeO₃-type distortion (right). (b) An AFM image of an EGTO film with $x = 0.35$. Clear 4-Å high steps and atomically flat terraces are seen. (c) XRD patterns around (002) peaks for EGTO thin films with various x , including undoped ($x = 0$) ETO thin film. Black triangles indicate EGTO film peaks. (d) Reciprocal space map around the (103) peak for the EGTO thin film with $x = 0.35$.

peculiar properties originating from the exchange coupling between the titanium t_{2g} -electrons and europium $4f$ moments. For bulk crystals, it has been elucidated that more than 7% doping of lanthanum or gadolinium into ETO induces ferromagnetic ordering via an exchange interaction mediated with conduction t_{2g} -electrons [22,29]. Regarding the lightly doped thin films, a previous work [26] reports that lanthanum-doped ETO thin films ($\text{La} < 1\%$) with a high crystalline quality can be grown on SrTiO₃ substrates by gas-source molecular beam epitaxy (MBE), exhibiting a maximum mobility over $3200 \text{ cm}^2 \text{ V}^{-1} \text{ s}^{-1}$ at 2 K. In such high-mobility films, clear Shubnikov-de Haas oscillations are observed at the forced ferromagnetic states under a magnetic field exceeding 3 T [26]. Besides such quantum transport phenomena, this high-mobility ETO is an excellent platform to study the anomalous Hall effect originating from the topology of the band structure [23,24,28,30,31]. In addition to a lightly doped system, the physical properties of heavily doped thin films of Eu_{1-x}La_xTiO₃ (ELTO) ($0 \leq x \leq 1$) on (LaAlO₃)_{0.3}(SrAl_{0.5}Ta_{0.5}O₃)_{0.7} (LSAT) substrates have also been reported [27], where localized Eu²⁺ moments undergo a magnetic transition from an antiferromagnetic state to a ferromagnetic state ($x \sim 0.1$) and then to a paramagnetic state ($x \sim 0.7$) with a signature of electron correlation enhancement with the filling x in the transport properties. It is noteworthy that as the lanthanum content increases in Eu_{1-x}La_xTiO₃, the long-range magnetic ordering for Eu²⁺ moments is weakened due to the spinless nature of La³⁺ ($4f^0$) ions embedded in the spin-full ($4f^7$) Eu²⁺ sublattice.

From the viewpoint of the A-site magnetic moment, a solid solution of Eu_{1-x}Gd_xTiO₃ is an intriguing system that enables us to control the filling of titanium t_{2g} -electrons embedded in

the $4f^7$ spin A-site sublattice consisting of Eu²⁺ ($4f^7$) and Gd³⁺ ($4f^7$). Despite an interest in the interplay between the correlated electron of the t_{2g} orbital and the large magnetic moment of the $4f^7$ state, there have been few reports that examine the physical properties of Eu_{1-x}Gd_xTiO₃, such as polycrystalline bulk crystals only with $x = 0.5$ and 0.7 [22] or lightly doped epitaxial thin films on STO substrates with $x \leq 0.09$ [28].

In this work, transport and magnetic properties are studied for EGTO high-quality thin films ($x = 0.1$ to 0.55) grown on LSAT substrates by gas-source MBE. The properties are compared with those of Sr_{1-x}La_xTiO₃ and Eu_{1-x}La_xTiO₃. As for the transport properties, EGTO films show a metallic behavior with temperature-squared (T^2) resistivity. This can be regarded as typical behavior of a Fermi liquid. The T^2 slope (A) values of resistivity, which are known to be in proportion to the square of the electronic specific heat coefficient γ [2,32,33], are considerably larger for EGTO thin films than those for Sr_{1-x}La_xTiO₃ and Eu_{1-x}La_xTiO₃, indicating stronger electron correlation in EGTO. As for the magnetic properties, the Eu_{1-x}Gd_xTiO₃ thin films with $x = 0.1$ to 0.55 show ferromagnetic ordering below the T_C that increases up to $x = 0.35$ and suddenly decreases around $x = 0.55$. We attribute it to the fact that the conduction electrons in EGTO begin to become less itinerant due to the enhancement of electron correlation and, accordingly, the Ruderman-Kittel-Kasuya-Yoshida (RKKY) interaction gets weaker from $x = 0.35$ to 0.5 [22]. We also discuss the filling dependence of the T_C of EGTO and ELTO, taking the strength of electron correlation and the presence (absence) of magnetic moment on gadolinium (lanthanum) into account.

II. EXPERIMENT

Epitaxial thin films of solid solution, EGTO, were grown on a (001) LSAT substrate ($a = 3.868 \text{ \AA}$) by a gas-source MBE system [34], the details of which are described in our previous work [26,28]. The thickness was designed to be $\sim 35 \text{ nm}$. Temperature of the LSAT substrate was heated to $1000 \text{ }^\circ\text{C}$ for the deposition of EGTO films. The EGTO films were grown in a reductive atmosphere; but, contrary to the SrTiO₃ substrate, the LSAT substrate is robust against oxygen deficiency, and the ozone annealing process [26,28] was not necessary. We also fabricated 20-nm thick ELTO thin films on an LSAT substrate for comparison using the same procedure. The methods to analyze the physical properties such as structure, transport, and magnetism are also described in our previous work [28].

III. RESULTS AND DISCUSSION

The structural characterization results for EGTO thin films are summarized in Fig. 1. Figure 1(b) shows a typical atomic force microscope (AFM) image for an EGTO thin film with $x = 0.35$ exhibiting a smooth surface morphology consisting of 4-Å (= one unit cell) steps and atomically flat terraces. X-ray diffraction (XRD) 2θ - θ scans for EGTO films with x from 0 to 0.55 are shown in Fig. 1(c). Sharp (002) film peaks are observed in all XRD patterns with clear Laue fringes, indicating the high crystalline quality. The less-intense peak

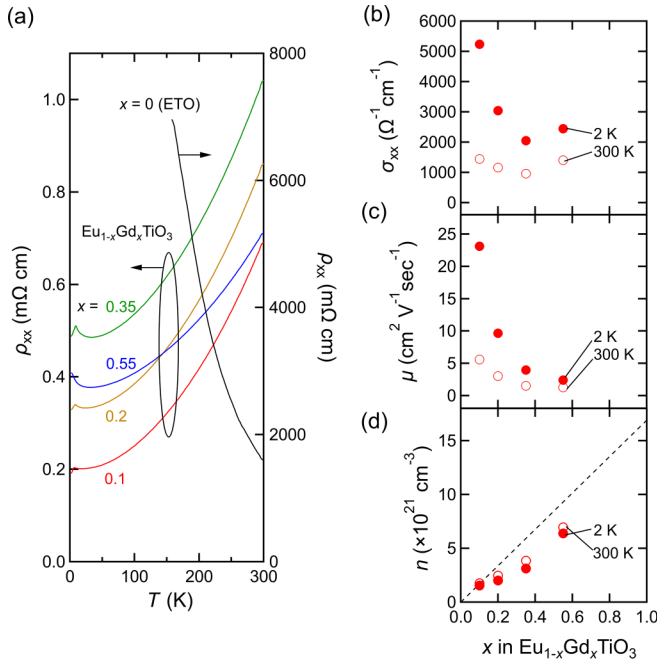


FIG. 2. Electrical transport properties of EGTO thin films grown on LSAT substrates. (a) Temperature dependence of longitudinal resistivity ρ_{xx} with various x for doped EGTO thin films (left axis) and undoped ETO thin films (right axis). (b)–(d) Filling (x) dependence of (b) longitudinal conductivity σ_{xx} , (c) mobility μ , and (d) carrier density n at 2 K (solid circles) and 300 K (open circles). The dashed line in (d) indicates the donor activation ratio of 100%.

with smeared Laue fringes for the $x = 0.55$ sample is due to crystalline disorder presumably originating from the unstable Ti^{3+} valence state in EGTO. All the EGTO thin films are coherently grown on LSAT substrates as confirmed by the reciprocal space mapping results, an example of which is shown for $x = 0.35$ in Fig. 1(d). We note that satellite peaks around the (103) peak correspond to Laue fringes. From these results, lattice constants are deduced as $a = 3.868 \text{ \AA}$ and $c = 3.901 \text{ \AA}$, resulting in a tetragonality of $c/a = 1.009$ with a compressive strain. As seen for the peak position in Fig. 1(c), c decreases from 3.931 \AA ($x = 0$) to 3.901 \AA ($x = 0.35$), and then increases to 3.909 \AA ($x = 0.55$). Such a trend is consistent with that for bulk or film solid solution systems [10,36], where the cell volume deviates to the smaller side via Vegard's law, presumably due to the compensating two factors of average r_A and titanium ion size with a $3d^x$ -electron configuration (see Supplemental Material Fig. S1 [35] and Refs. [10,12,27,36] therein). It is noted that we have not been able to prepare epitaxial thin films with high crystallinity for $x \geq 0.6$, where a rough surface is observed in AFM images and a pyrochlore impurity phase appears in XRD patterns.

Next, we discuss the fundamental transport properties. Figure 2(a) shows the temperature (T) dependence of longitudinal resistivity (ρ_{xx}) for EGTO thin films. All ρ_{xx} - T curves show metallic behavior with kink structures at $\sim 5 \text{ K}$ due to magnetic ordering. Filling dependences of longitudinal conductivity σ_{xx} , mobility μ , and carrier density n at 2 K and 300 K are shown in Fig. 2(b)–2(d). Mobility shows a systematic decrement with band filling, predominantly due

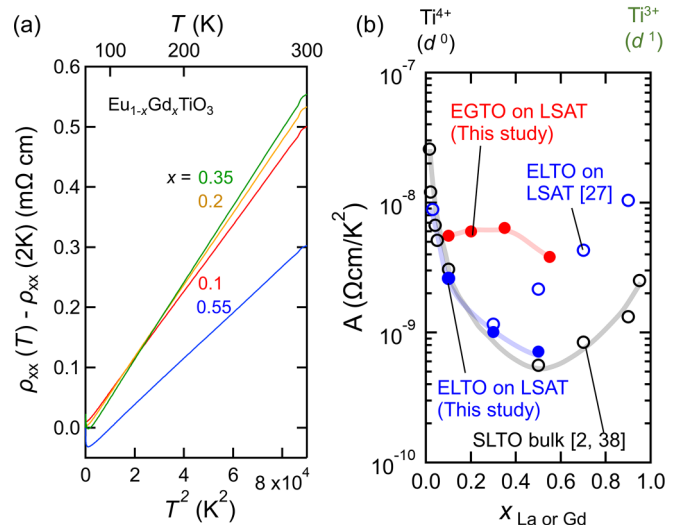


FIG. 3. (a) Resistivity, $\rho_{xx}(T) - \rho_{xx}(2 \text{ K})$, versus T^2 for EGTO thin films with various x . (b) Filling dependence of the T^2 coefficient A of resistivity in $\rho_{xx}(T) = \rho_0 + AT^2$ for EGTO (red filled circles) in comparison with those for ELTO (blue filled circles, grown in this work, and blue open circles [27]) thin films on LSAT substrates, as well as for SLTO bulk crystals (open black circles [2,38]).

to enhanced impurity scattering. In comparison with the data for ELTO (see Supplemental Material Fig. S2 [35]), the value of μ is much smaller for EGTO, suggesting stronger impurity scattering and electron correlation due to local lattice distortion, as discussed later. Carrier density increases with band filling as expected, while the activation ratio of the gadolinium donor is slightly lower than 100% for larger x , which is presumably originating from carrier trapping at some lattice defects. We note σ_{xx} does not decrease monotonically, but it takes a minimum value at $x = 0.35$. This is due to the competition between the mobility decrement and the carrier density increment. Comparison with the data for ELTO thin films is given in Supplemental Material Fig. S2 [35].

We now discuss the evolution of electron correlation in EGTO thin films on the basis of the transport and magnetic properties. Figure 3(a) shows the T^2 dependence of resistivity, $\rho_{xx}(T) - \rho_{xx}(2 \text{ K})$, for EGTO thin films. The data for all these films are well consistent with the typical Fermi liquid-like behavior: $\rho_{xx}(T) = \rho_0 + AT^2$ at a wide temperature range up to 300 K, where the coefficient A represents the strength of the electron correlation. We note that the T^2 dependence of resistivity predominantly originates from the electron-electron scattering process, while the impurity scattering is temperature independent and appears as the residual resistivity at the lowest temperature [37]. Figure 3(b) shows the filling dependence of the coefficient A for EGTO thin films in comparison with ELTO thin films grown in this work as well as the data in the literature for ELTO thin films on LSAT substrates [27] and $\text{Sr}_{1-x}\text{La}_x\text{TiO}_3$ (SLTO) bulk crystals [2,38], all of which employ La^{3+} as the donor with a larger ionic radius than Gd^{3+} . The coefficient A for ELTO or SLTO shows downward convex. For the larger x side, A increases with x due to the enhancement of electron correlation toward $x = 1$ (LaTiO_3 as a typical Mott insulator with $3d^1$ on Ti^{3+}). The region around

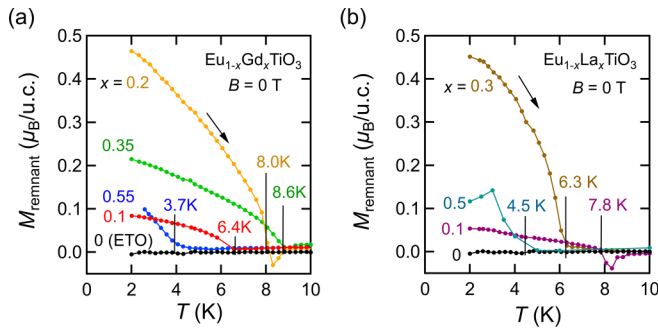


FIG. 4. Temperature dependence of remnant magnetization for (a) EGTO and (b) ELTO thin films measured under $B = 0$ T. The remnant magnetization was induced by applying a 9-T magnetic field at $T = 2$ K along the out-of-plane axis, then the temperature was raised from 2 K. As for ELTO ($x = 0.5$), in order to confirm the presence of magnetization, the M - H (H : magnetic field) curves were measured for respective temperatures, and magnetization (0 T) was plotted. The black arrows indicate the direction of the temperature sweep. The vertical black lines indicate the T_C where remnant magnetization disappears.

$x = 0$ far away from the correlated electron system also shows a very large value for coefficient A . This is because the dilute carrier doped semiconductor shows high resistivity due to its small carrier density, which dominantly contributes to a larger slope in the temperature dependence of resistivity. The coefficient A for EGTO is $\sim 5 \times 10^{-9} \Omega\text{-cm K}^{-2}$ for $x = 0.1$ to 0.55 [Fig. 3(b), red circles], which is much larger than those for ELTO and SLTO, indicating the stronger electron correlation in EGTO. It is due to the smaller ionic radius of Gd^{3+} than La^{3+} , which makes the lattice distortion or tilting of the TiO_6 octahedra larger and the bond angle of Ti-O-Ti smaller [7]. This smaller bond angle in EGTO makes the transfer integral (one-electron bandwidth) for the titanium t_{2g} conduction electron smaller [8,9], resulting in the enhancement of electron correlation.

As for the magnetic property, all EGTO thin films with $x = 0.1$ to 0.55 show ferromagnetic transitions. Figure 4(a) and (b), respectively, show the temperature dependence of remnant magnetization (M_{remnant}) for EGTO and ELTO thin films. To deduce the T_C , we take the temperature where the M_{remnant} disappears in the warming process under $B = 0$ T after fully magnetizing under $B = 9$ T at $T = 2$ K. All EGTO and ELTO thin films have a nonzero M_{remnant} at $T = 2$ K due to the ferromagnetic ordering, while ETO thin films ($x = 0$) show no remnant magnetization due to the antiferromagnetic ground state.

Figure 5 shows the filling dependence of the T_C and T_N for various samples of EGTO (red symbols) and ELTO (blue symbols). The data with filled symbols are our own thin-film data, including gadolinium- or lanthanum-doped ETO thin films on STO substrates with a dilute doping of $x \leq 0.1$ [28] and ELTO thin films on an LSAT substrate ($x = 0.1, 0.3$, and 0.5). For low doped samples with $x \leq 0.07$, both EGTO and ELTO show antiferromagnetic ordering: $T_N = 5.5$ K for EGTO; while for ELTO, the T_N gradually decreases with x to $T_N = 3.5$ K. As discussed in our previous work [28], this is ascribed to the presence or absence of a magnetic

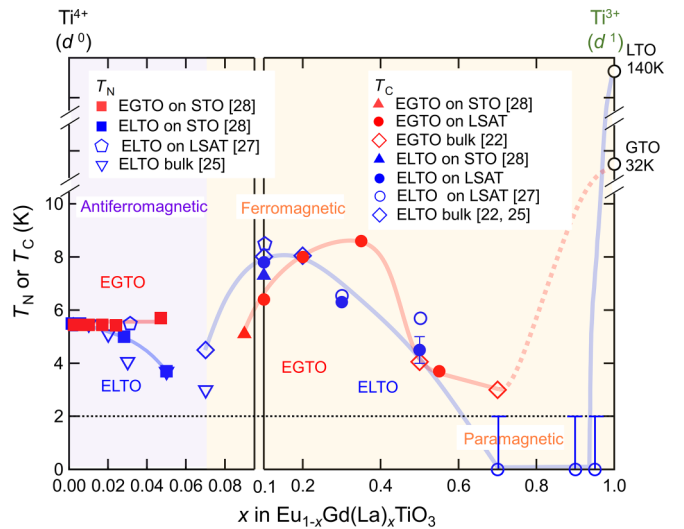


FIG. 5. Filling dependence of ferromagnetic (antiferromagnetic) transition temperature T_C (T_N) for EGTO (red symbols) and ELTO (blue symbols). The filled symbols represent the thin-film samples grown in the current work and our previous work [28]. Open symbols are indicative of the data in the literature, including bulk crystals [22,25] and ELTO thin films on LSAT substrates [27]. Open circles at $x = 1$ indicate the T_C for LaTiO_3 (140 K) and GdTiO_3 (32 K) bulk single crystals [18]. The horizontal dashed line at $T = 2$ K represents the lowest temperature attained in our magnetization measurement.

moment for the dopant elements; nonmagnetic La^{3+} disturbs the long-range antiferromagnetic ordering in ETO, while it can be kept robust in the case of Gd^{3+} doping, which has the same magnetic moment of the $4f^7$ state of Eu^{2+} . Above $x = 0.07$, EGTO and ELTO both show the transition from an antiferromagnetic state to a ferromagnetic state. Such a magnetic transition plausibly originates from a RKKY interaction, where titanium t_{2g} conduction electrons mediate the ferromagnetic ordering of localized $4f$ spins on A-sites [22].

Above $x = 0.07$, the T_C of both EGTO and ELTO shows a similar behavior of upward convex against the filling x . However, there are several important differences. Here, we explain them qualitatively while taking into account the RKKY interaction, strength of electron correlation, and the presence (absence) of a magnetic moment on the gadolinium (lanthanum) site. As for ELTO, its T_C increases from 4.5 K at $x = 0.07$ to 8 K at $x = 0.2$, which can be ascribed to the enhanced ferromagnetic RKKY interaction due to the increment in carrier density. Above $x = 0.2$, the T_C decreases and, finally, the ferromagnetic order disappears at $\sim 0.5 < x < 0.7$, even though the carrier density is still increasing. We attribute this suppression of ferromagnetism to a dilution of the europium $4f$ moment by a substitution with nonmagnetic lanthanum. In contrast, the T_C of EGTO increases as the filling x increases, from 5.1 K at $x = 0.09$ to 8.6 K at 0.35. It is notable that, at $x = 0.1$, the T_C for EGTO is lower than ELTO by 1 or 2 K despite of our naive expectation that gadolinium substitution will cause a higher T_C than ELTO because of the $4f^7$ moment on Gd^{3+} . The dominant factor for a suppressed T_C seems to be the stronger electron correlation in EGTO than in ELTO, as demonstrated by Fig. 3; the conduction electron in distorted

EGTO is less itinerant than in ELTO, causing a weaker RKKY interaction. Thus, the T_C for EGTO suddenly drops from 8.6 K at $x = 0.35$ to 4 K at $x = 0.5$ and furthermore decreases to 3 K at $x = 0.7$. This indicates that conduction electrons in EGTO begin to be increasingly affected by increasing electron correlation above $x = 0.5$, and the RKKY interaction is getting weaker. One may expect that the suppressed T_C at $x = 0.5$ may be caused by the conventional electron localization effect due to carrier trapping at impurity sites, which should weaken the RKKY interaction. However, we consider that the electron correlation plays a dominant role in suppression of the T_C because the apparent carrier density at the lowest temperature (2 K) does not decrease much compared with that at 300 K, and increases almost linearly from $x = 0.35$ to 0.5 without the distinct carrier trapping effect, while the enhancement of resistivity occurs due to the enhanced electron correlation as well as impurity scattering. It is noteworthy that the T_C at $x = 0.5$ is comparable between EGTO and ELTO even though lanthanum doping introduces spin vacancies in A-sites. This indicates that the electron correlation effect dominates the magnetic transition temperature in the EGTO system. Unlike the paramagnetic state for ELTO with $x \geq 0.7$ [27], the ferromagnetism survives in EGTO due to the $4f^7$ moment on Gd^{3+} [22]. Regarding the region of $x = 0.7$ to 1, the change in the T_C for EGTO remains unknown, and further studies are needed to clarify the behavior on the verge of the Mott transition.

IV. CONCLUSIONS

In summary, we have investigated the magnetic and transport properties of $Eu_{1-x}Gd_xTiO_3$ thin films with $x = 0$ to 0.55 grown by gas-source MBE. The transport measurement revealed that all the metallic EGTO thin films show a Fermi liquid-like behavior with typical temperature dependence, such as $\rho_{xx}(T) = \rho_0 + AT^2$. The coefficient A for our EGTO thin films is larger than that for $Sr_{1-x}La_xTiO_3$ and $Eu_{1-x}La_xTiO_3$, indicating the stronger electron correlation in EGTO due to the smaller ionic radius of Gd^{3+} than La^{3+} . As for magnetic properties, EGTO thin films with $x = 0.1$ to 0.55 exhibited ferromagnetic ordering due to an RKKY interaction among localized $4f^7$ magnetic moments. The influence of electron correlation was observed as a suppression of the T_C seen in the filling dependence of the T_C for EGTO thin films compared to ELTO. These findings indicate the electron correlation has a crucial impact not only on transport properties, but also on exchange interactions among localized $4f^7$ magnetic moments mediated with conduction t_{2g} -electrons.

ACKNOWLEDGMENTS

We thank Naoto Nagaosa for fruitful discussion. This research was supported by Japan Society for the Promotion of Science (JSPS) Valid Funder (Grant No. 22H04958).

-
- [1] M. Imada, A. Fujimori, and Y. Tokura, *Rev. Mod. Phys.* **70**, 1039 (1998).
 - [2] Y. Tokura, Y. Taguchi, Y. Okada, Y. Fujishima, T. Arima, K. Kumagai, and Y. Iye, *Phys. Rev. Lett.* **70**, 2126 (1993).
 - [3] C. Eylem, H. L. Ju, B. W. Eichhorn, and R. L. Greene, *J. Solid State Chem.* **114**, 164 (1995).
 - [4] M. Heinrich, H. A. Krug von Nidda, V. Fritsch, and A. Loidl, *Phys. Rev. B* **63**, 193103 (2001).
 - [5] S. Das, A. Poddar, and B. Roy, *J. Alloys Compd.* **358**, 17 (2003).
 - [6] H. Kim, P. B. Marshall, K. Ahadi, T. E. Mates, E. Mikheev, and S. Stemmer, *Phys. Rev. Lett.* **119**, 186803 (2017).
 - [7] D. A. Maclean, H.-N. Ng, and J. E. Greedan, *J. Solid State Chem.* **30**, 35 (1979).
 - [8] T. Katsufuji, Y. Okimoto, and Y. Tokura, *Phys. Rev. Lett.* **75**, 3497 (1995).
 - [9] Y. Okimoto, T. Katsufuji, Y. Okada, T. Arima, and Y. Tokura, *Phys. Rev. B* **51**, 9581 (1995).
 - [10] C. C. Hays, J. S. Zhou, J. T. Markert, and J. B. Goodenough, *Phys. Rev. B* **60**, 10367 (1999).
 - [11] D. A. Crandles, T. Timusk, J. D. Garrett, and J. E. Greedan, *Physica C* **201**, 407 (1992).
 - [12] P. Moetakef, D. G. Ouellette, J. Y. Zhang, T. A. Cain, S. J. Allen, and S. Stemmer, *J. Cryst. Growth* **355**, 166 (2012).
 - [13] M. N. Grisolia, F. Y. Bruno, D. Sando, H. J. Zhao, E. Jacquet, X. M. Chen, L. Bellaiche, A. Barthélemy, and M. Bibes, *Appl. Phys. Lett.* **105**, 172402 (2014).
 - [14] P. Moetakef and T. A. Cain, *Thin Solid Films* **583**, 129 (2015).
 - [15] J. E. Greedan, *J. Less-Common Met.* **111**, 335 (1985).
 - [16] T. Katsufuji, Y. Taguchi, and Y. Tokura, *Phys. Rev. B* **56**, 10145 (1997).
 - [17] M. Mochizuki and M. Imada, *New J. Phys.* **6**, 154 (2004).
 - [18] H. D. Zhou and J. B. Goodenough, *J. Phys. Condens. Matter* **17**, 7395 (2005).
 - [19] T. R. McGuire, M. W. Shafer, R. J. Joenk, H. A. Alperin, and S. J. Pickart, *J. Appl. Phys.* **37**, 981 (1966).
 - [20] C. L. Chien, S. DeBenedetti, F. De, and S. Barros, *Phys. Rev. B* **10**, 3913 (1974).
 - [21] A. P. Petrović, Y. Kato, S. S. Sunku, T. Ito, P. Sengupta, L. Spalek, M. Shimuta, T. Katsufuji, C. D. Batista, S. S. Saxena, and C. Panagopoulos, *Phys. Rev. B* **87**, 064103 (2013).
 - [22] T. Katsufuji and Y. Tokura, *Phys. Rev. B* **60**, R15021 (1999).
 - [23] K. S. Takahashi, M. Onoda, M. Kawasaki, N. Nagaosa, and Y. Tokura, *Phys. Rev. Lett.* **103**, 057204 (2009).
 - [24] K. S. Takahashi, H. Ishizuka, T. Murata, Q. Y. Wang, Y. Tokura, N. Nagaosa, and M. Kawasaki, *Sci. Adv.* **4**, eaar7880 (2018).
 - [25] Y. Tomioka, T. Ito, and A. Sawa, *J. Phys. Soc. Jpn.* **87**, 094716 (2018).
 - [26] K. Maruhashi, K. S. Takahashi, M. S. Bahramy, S. Shimizu, R. Kurihara, A. Miyake, M. Tokunaga, Y. Tokura, and M. Kawasaki, *Adv. Mater.* **32**, 1908315 (2020).
 - [27] H. Shin, C. Liu, F. Li, R. Sutarto, B. A. Davidson, and K. Zou, *Phys. Rev. B* **101**, 214105 (2020).

- [28] N. Takahara, K. S. Takahashi, K. Maruhashi, Y. Tokura, and M. Kawasaki, *APL Mater.* **11**, 031101 (2023).
- [29] Z. Gui and A. Janotti, *Phys. Rev. Lett.* **123**, 127201 (2019).
- [30] K. Ahadi, L. Galletti, and S. Stemmer, *Appl. Phys. Lett.* **111**, 172403 (2017).
- [31] K. Ahadi, Z. Gui, Z. Porter, J. W. Lynn, Z. Xu, S. D. Wilson, A. Janotti, and S. Stemmer, *APL Mater.* **6**, 056105 (2018).
- [32] K. Kadowaki and S. B. Woods, *Solid State Commun.* **58**, 507 (1986).
- [33] K. Miyake, T. Matsuura, and C. M. Varma, *Solid State Commun.* **71**, 1149 (1989).
- [34] B. Jalan, R. Engel-Herbert, N. J. Wright, and S. Stemmer, *J. Vac. Sci. Technol. A* **27**, 461 (2009).
- [35] See Supplemental Material at <http://link.aps.org/supplemental/10.1103/PhysRevB.108.125138> for the filling dependence of cell volume and transport properties for ELTO thin films.
- [36] Y. Zhang, K. Sugo, H. J. Cho, and H. Ohta, *J. Appl. Phys.* **126**, 075104 (2019).
- [37] J. M. Ziman, *Electrons and Phonons: The Theory of Transport Phenomena in Solids* (Oxford University Press, Oxford, 2001).
- [38] T. Okuda, K. Nakanishi, S. Miyasaka, and Y. Tokura, *Phys. Rev. B* **63**, 113104 (2001).